# A study of hyperons in nuclear matter based on chiral effective field theory

J. Haidenbauer[a], Ulf-G. Meißner[b,a]

[a] *Institute for Advanced Simulation, Institut für Kernphysik and Jülich Center for Hadron Physics, Forschungszentrum Jülich, D-52425 Jülich, Germany*

[b] *Helmholtz Institut für Strahlen- und Kernphysik and Bethe Center for Theoretical Physics, Universität Bonn, D-53115 Bonn, Germany*



**Abstract**

The in-medium properties of a hyperon-nucleon potential, derived within chiral effective field theory and fitted to $\Lambda N$ and $\Sigma N$ scattering data, are investigated. Results for the single-particle potentials of the $\Lambda$ and $\Sigma$ hyperons in nuclear matter are reported, based on a conventional $G$-matrix calculation. The $\Sigma$-nuclear potential is found to be repulsive, in agreement with phenomenological information. A weak $\Lambda$-nuclear spin-orbit interaction can be achieved by an appropriate adjustment of a low-energy constant corresponding to an antisymmetric $\Lambda N$–$\Sigma N$ spin-orbit interaction that arises at next-to-leading order in the effective field theory approach.

*Keywords:* $YN$ interaction, chiral effective field theory, $G$-matrix, hyperon single-particle potential, spin-orbit interaction
*PACS:* 13.75.Ev,12.39.Fe,14.20.Jn,21.65.-f

## 1. Introduction

Chiral effective field theory (EFT) as proposed in the pioneering works of Weinberg [1, 2] is a powerful tool for the derivation of baryonic forces. In this scheme there is an underlying power counting which allows one to improve calculations systematically by going to higher orders in a perturbative expansion. In addition, it is possible to derive two- and corresponding three-body and even four-body forces as well as external current operators in a consistent way. For a review, see e.g. Ref. [3].

Recently, a hyperon-nucleon ($YN$) interaction has been derived up to next-to-leading order (NLO) in chiral EFT by the Jülich-Bonn-Munich group [4]. At that order there are contributions from one- and two-pseudoscalar-meson exchange diagrams (involving $\pi$, $K$, $\eta$) and from four-baryon contact terms without and with two derivatives. SU(3) flavor symmetry is imposed for constructing the $YN$ interaction. The assumed SU(3) symmetry allows us to fix all the coupling constants at the various meson-baryon vertices, and it reduces the number of free parameters which arise within the EFT approach in form of low-energy constants (LECs) associated with the aforementioned contact terms. In the actual calculation the SU(3) symmetry is broken, however, because the physical masses of the involved mesons and octet baryons ($N$, $\Lambda$, $\Sigma$, $\Xi$) are used. With this interaction an excellent reproduction of available low-energy $\Lambda N$ and $\Sigma N$ scattering data could be achieved as reflected in a total $\chi^2$ of about 16 for the 36 data points included in the fit [4]. Thus, the description of the $YN$ system at NLO is on the same level of quality as by the most advanced meson-exchange $YN$ interactions.

In the present work we investigate the properties of our $YN$ interactions in nuclear matter. Specifically, we report results for the single particle (s.p.) potential of the $\Lambda$ and $\Sigma$ hyperons in nuclear matter obtained in a conventional $G$-matrix calculation based on the standard (gap) choice for the intermediate spectrum. Of specific interest for us are two long-standing issues that have been discussed extensively in the literature, namely the repulsive nature of the $\Sigma$-nucleus potential and the weak $\Lambda$-nucleus spin-orbit interaction. For recent overviews of strangeness nuclear physics see Refs. [5, 6, 7].

It is now generally accepted that the $\Sigma$-nuclear potential is repulsive [8]. Phenomenological evidence comes, for example, from recently measured $(\pi^-, K^+)$ inclusive spectra related to $\Sigma^-$-formation in heavy nuclei [9, 10] which suggest a repulsive $\Sigma$-nucleus potential [11, 12]. But also the theoretical interpretation of measured level shifts and widths of $\Sigma^-$ atoms [13, 14] requires a repulsive component of the $\Sigma$-nucleus potential. Microscopic models of the $YN$

interaction, fitted to $\Lambda N$ and $\Sigma N$ scattering data, often fail to produce a repulsive $\Sigma$-nuclear potential. Specifically, for models based on meson-exchange dynamics it is rather difficult to obtain such a repulsion as is witnessed by results of $G$-matrix calculations for various generations of the Nijmegen $YN$ potential [15, 16, 17, 18]. Only the most recent version [19] could overcome this difficulty [20, 21] - but at the expense of a noticeable increase in the achieved $\chi^2$. The situation is different for $YN$ potentials derived within a constituent quark model [22]. Here, the interaction in the $^3S_1$ partial wave of the $I = 3/2$ $\Sigma N$ channel is always strongly repulsive due to Pauli blocking effects on the quark level [22, 23], and as direct consequence of this feature a repulsive $\Sigma$-nuclear potential is obtained in pertinent $G$-matrix calculations.

Interestingly, our leading order (LO) $YN$ interaction, published in 2006 [24], predicted also a repulsive $^3S_1$ partial wave. Calculations of the $\Sigma$ s.p. potential, performed by Kohno with a low-energy equivalent representation [25], revealed that this interaction produces indeed a repulsive $\Sigma$-nuclear potential. The LO interaction involves only five contact terms and the LECs associated with them were determined in a fit to the low-energy $\Lambda N$ and $\Sigma N$ cross sections. No attention was paid to the sign of the $I = 3/2$ $\Sigma N$ amplitude in the $^3S_1$ partial wave. In the course of constructing the EFT interaction [4] up to NLO (which involves altogether 13 LECs in the $S$ waves and the $S$–$D$ transitions) it turned out that the available $YN$ scattering data could be fitted equally well with an attractive or a repulsive interaction in the $^3S_1$ partial wave of the $I = 3/2$ $\Sigma N$ channel. For the reasons discussed above, the repulsive solution was adopted. The resulting interaction produces a moderately repulsive $^3S_1$ phase shift as can be seen in Fig. 9 of Ref. [4]. First $G$-matrix calculations for this interaction will be reported in the present work. It turns out that a repulsive $\Sigma$-nuclear potential is predicted.

Hypernuclear spectra provide clear indication for a rather weak $\Lambda$-nucleus spin-orbit potential [5, 6, 7]. Apparently, also this feature is difficult to reproduce with microscopic models of the $YN$ interaction. In particular, meson-exchange potentials tend to grossly overestimate the spin-orbit force, judging from applications of various Nijmegen models in the studies presented in Refs. [26] and [27, 28]. Calculations based on $YN$ interactions derived in the quark model lead to (partially) more promising results [22, 29]. According to the discussion of the strength of the spin-orbit potential in Refs. [22, 23, 30], done on the level of the Scheerbaum factor [31] calculated from the $G$-matrix, there is a sizeable antisymmetric spin-orbit component generated from the quark model which cancels to a large extent the symmetric component in the $\Lambda N$ isospin $I = 1/2$ channel so that an overall weak spin-orbit potential is achieved.

The aforementioned work by Kohno [25] provides also results for the Scheerbaum factor for our LO $YN$ potential. The predicted value was found to be fairly small and – somewhat surprisingly – of opposite sign as compared to results from standard potential models. At leading order there is no contact term that would give rise to an antisymmetric spin-orbit component. Thus, the result at LO is a pure prediction based on the dynamics generated by pseudoscalar meson exchange. This is different at NLO where such a contact term occurs and facilitates $^1P_1$–$^3P_1$ transitions in the coupled ($I = 1/2$) $\Lambda N$–$\Sigma N$ system [4]. Since the corresponding LEC could not be pinned down by a fit to the existing $\Lambda N$ and $\Sigma N$ scattering data it was simply put to zero in Ref. [4]. However, it is interesting to see whether that LEC can be fixed now from a study of the properties of the $\Lambda$ hyperon in nuclear matter and, specifically, whether it can be utilized to achieve a weak $\Lambda$-nuclear spin-orbit potential. This is indeed the case as will be demonstrated in the present work.

Note that the same issues have been addressed by Kaiser and Weise [32, 33, 34, 35] within an approach similar to ours, but on a perturbative level. It was found that the iterated (second order) one-pion exchange (with $\Lambda$ and $\Sigma$ intermediate states) gives rise to a repulsive $\Sigma$-nuclear potential. Note that dimensional regularization has been employed to extract the genuine long-range components. Second-order pion exchange plays also a decisive role for the spin-orbit force, where it is argued that its contribution counterbalances the short-range components due to the scalar and vector mean fields to a large extent in case of the $\Lambda$ and, accordingly, leads to a small net result for the $\Lambda$-nuclear spin-orbit force. The same mechanism is at work for the $\Sigma$-nuclear spin-orbit coupling [34]. An analogous calculation where, in addition, contributions involving the decuplet baryons $\Delta$ and $\Sigma^*$ were considered [36] led to the same conclusions concerning the $\Lambda$-nuclear spin-orbit force.

The paper is structured as follows: In Sect. 2 the formalism employed for evaluating the $G$-matrix is outlined. Sect. 3 provides a basic introduction to our EFT $YN$ potentials. Specifically, the implementation of the antisymmetric spin-orbit force and its impact on the $\Lambda N$ and $\Sigma N$ results are discussed. Results of our calculation are presented and analysed in Sect. 4. Besides those based on our chiral EFT interactions, predictions for three meson-exchange potentials (developed by the Jülich and Nijmegen groups, respectively) are included for illustration purposes. The paper ends with a short summary.

## 2. Formalism for the G-matrix calculation

The standard formalism for the treatment of a hyperon in nuclear matter is the conventional Brueckner theory. For convenience we summarize below the essential formulae employed in our calculation. A more detailed description can be found in Ref. [37], see also [16].

We consider a $\Lambda$ or $\Sigma$ hyperon with momentum $\mathbf{p}_Y$ in nuclear matter of density $\rho = (2/3\pi^2)\, k_F^3$, where $k_F$ denotes the Fermi momentum of nuclear matter. In order to determine the properties of those hyperons we employ the Brueckner reaction-matrix formalism as discussed in Refs. [38, 39]. The $YN$ reaction matrix, $G_{YN}$, is defined by the Bethe-Goldstone equation

$$\langle YN|G_{YN}(\zeta)|YN\rangle = \langle YN|V|YN\rangle + \sum_{Y'N} \langle YN|V|Y'N\rangle \, \langle Y'N|\frac{Q}{\zeta - H_0}|Y'N\rangle \, \langle Y'N|G_{YN}(\zeta)|YN\rangle, \tag{1}$$

with $Y$, $Y' = \Lambda, \Sigma$. Here, $Q$ is the Pauli projection operator, which excludes those intermediate $YN$ states with the nucleon inside the Fermi sea. The starting energy $\zeta$ for an initial $YN$ state with momenta $\mathbf{p}_Y$, $\mathbf{p}_N$ is given by

$$\zeta = E_Y(p_Y) + E_N(p_N), \tag{2}$$

where the s.p. energy $E_\alpha(p_\alpha)$ ($\alpha = \Lambda, \Sigma, N$) includes not only the (nonrelativistic) kinetic energy and the particle mass but in addition the s.p. potential $U_\alpha(p_\alpha)$:

$$E_\alpha(p_\alpha) = M_\alpha + \frac{p_\alpha^2}{2M_\alpha} + U_\alpha(p_\alpha). \tag{3}$$

Here and in the following, $p_Y$ denotes the modulus of $\mathbf{p}_Y$, etc.

In practice, the Bethe-Goldstone equation is solved for a given $Y$ momentum $\mathbf{p}_Y$ and relative momentum $\mathbf{p}$ of the initial $\Lambda N$ or $\Sigma N$ state. For that purpose we re-write the energy denominator in Eq. (1) in the form

$$\begin{aligned} e_Y(k;K,\zeta) &= \langle \mathbf{k}_Y, \mathbf{k}_N|\frac{1}{\zeta - H_0}|\mathbf{k}_Y, \mathbf{k}_N\rangle \\ &= \left(\zeta - M_Y - M_N - \frac{k_Y^2}{2M_Y} - \frac{k_N^2}{2M_N} + \mathrm{i}\epsilon\right)^{-1} \\ &= \left(\zeta - M_Y - M_N - \frac{K^2}{2(M_Y + M_N)} - \frac{k^2}{2\mu_{YN}} + \mathrm{i}\epsilon\right)^{-1}, \end{aligned} \tag{4}$$

where we have introduced the total and relative momenta, $\mathbf{K}$ and $\mathbf{k}$, which are related to the $Y$ and $N$ momenta $\mathbf{k}_Y$ and $\mathbf{k}_N$ via

$$\mathbf{K} = \mathbf{k}_Y + \mathbf{k}_N, \qquad \mathbf{k} = \frac{M_N\mathbf{k}_Y - M_Y\mathbf{k}_N}{M_N + M_Y}, \tag{5}$$

The reduced mass in Eq. (4) is given by $\mu_{YN} \equiv M_Y M_N/(M_Y + M_N)$.

The square of the (conserved) total momentum, $\mathbf{K}^2$, can be written as

$$K^2 \equiv \mathbf{K}^2 = (1 + \xi_Y)^2(\mathbf{p}_Y - \mathbf{p})^2 \tag{6}$$

with $\xi_Y = M_N/M_Y$. Note that $e_Y$ depends via $K^2$ on the angle between $\mathbf{p}_Y$ and $\mathbf{p}$. Also the Pauli projection operator,

$$Q\left(k_N = |-\mathbf{k} + (1 + \xi_{Y'}^{-1})^{-1}\mathbf{K}|\right), \tag{7}$$

depends on the angle between the total momentum $\mathbf{K}$ and the relative momentum $\mathbf{k}$ of the intermediate $YN$ state. In order to facilitate a partial-wave decomposition (with regard to the total $YN$ angular momentum $\mathbf{J}$, with $\mathbf{J}$ the sum of the total spin $\mathbf{S}$ and the relative angular momentum $\mathbf{L}$: $\mathbf{J} = \mathbf{L} + \mathbf{S}$) it is common practice to approximate $K^2$ and $Q(k_N)$ by their angle-averaged values, evaluated for given $p_Y$, $p$ of the initial $YN$ state. These are given by

$$\begin{aligned}\overline{K^2} &= \overline{K^2}(p_Y,p)\\ &= \begin{cases}(1+\xi_Y)^2(p_Y^2+p^2), & \text{for}\quad \xi_Y p_Y+(1+\xi_Y)p\le k_F\\ (1+\xi_Y)^2(p_Y^2+p^2)+\frac{1}{2}(1+\xi_Y^{-1})[k_F^2-[\xi_Y p_Y+(1+\xi_Y)p]^2], & \text{otherwise}\,,\end{cases}\end{aligned} \tag{8}$$

$$\overline{Q}_{Y'}(k;p_Y,p)=\begin{cases}0, & \text{for}\quad k+\frac{\xi_{Y'}}{1+\xi_{Y'}}\sqrt{\overline{K^2}}\le k_F\\ 1, & \text{for}\quad |k-\frac{\xi_{Y'}}{1+\xi_{Y'}}\sqrt{\overline{K^2}}|>k_F\\ (1+\xi_{Y'}^{-1})\left[\left(k+\frac{\xi_{Y'}}{1+\xi_{Y'}}\sqrt{\overline{K^2}}\right)^2-k_F^2\right]/4k\sqrt{\overline{K^2}}, & \text{otherwise}\,.\end{cases} \tag{9}$$

When evaluating the starting energy $\zeta = E_Y(p_Y)+E_N(p_N)$ the nucleon momentum of the initial $YN$ state, $p_N$, is approximated by

$$p_N \approx \left[\frac{\xi_Y}{1+\xi_Y}\overline{K}^2+(1+\xi_Y)p^2-\xi_Y p_Y^2\right]^{1/2}\,. \tag{10}$$

The partial-wave expanded Bethe-Goldstone equation reads

$$\begin{aligned}G^{J,I_0}_{\alpha S'L',\alpha SL}(q,p;p_Y) &= V^{J,I_0}_{\alpha S'L',\alpha SL}(q,p)\\ &+ \sum_{\beta S''L''}\int_0^\infty \frac{k^2\,dk}{(2\pi)^3}\,V^{J,I_0}_{\alpha S'L',\beta S''L''}(q,k)\,\overline{Q}_\beta(k;p_Y,p)e_\beta(k;p_Y,p)\,G^{J,I_0}_{\beta S''L'',\alpha SL}(k,p;p_Y)\,,\end{aligned} \tag{11}$$

where $\alpha$ stands for $\Lambda$ or $\Sigma$ and $I_0$ is the total $YN$ isospin which can be $1/2$ or $3/2$.

The hyperon s.p. potential $U_Y$ is calculated from

$$U_Y(p_Y)=(1+\xi_Y)^3\sum_{I_0}\frac{2I_0+1}{2(2I_Y+1)}\sum_{JSL}(2J+1)\int_0^{p_{max}}\frac{p^2\,dp}{(2\pi)^3}\,W(p,p_Y)\,G^{J,I_0}_{YSL,YSL}(p,p;p_Y)\,, \tag{12}$$

where $p_{max}=(k_F+\xi_Y p_Y)/(1+\xi_Y)$. The weight function $W(p,p_Y)$ is given by

$$W(p,p_Y)=\begin{cases}1, & \text{for}\quad p\le\frac{k_F-\xi_Y p_Y}{1+\xi_Y},\\ 0, & \text{for}\quad |\xi_Y p_Y-(1+\xi_Y)p|>k_F,\\ \frac{k_F^2-[\xi_Y p_Y-(1+\xi_Y)p]^2}{4\xi_Y(1+\xi_Y)p_Y p}, & \text{otherwise}\,.\end{cases} \tag{13}$$

We evaluate the $\Lambda$ and $\Sigma$ s.p. potentials $U_\Lambda$ and $U_\Sigma$ self-consistently in the standard way for a fixed Fermi momentum $k_F$. In case of the $\Sigma$ hyperon we decompose the s.p. potential into an isoscalar and an isovector based on the parameterization [6]

$$U_\Sigma = U_\Sigma^0+\frac{1}{A}U_\Sigma^1\,\mathbf{t}_\Sigma\cdot\mathbf{T}_A\,. \tag{14}$$

Here, $\mathbf{t}_\Sigma$ and $\mathbf{T}_A$ are the isospin operators of the $\Sigma$ and the nucleus (with $A$ nucleons). The isoscalar and isovector components are given by $U_\Sigma^0=U_{\frac{3}{2}}+U_{\frac{1}{2}}$ and $U_\Sigma^1=U_{\frac{3}{2}}-2U_{\frac{1}{2}}$, respectively, where $U_{I_0}$ are the corresponding parts of the sum over $I_0$ in Eq. (12).

In case of the $\Sigma$ hyperon, the propagator in Eq. (4) can become singular if the $\Sigma$ s.p. potential is repulsive. We avoided the proper but technically involved treatment of this singularity by adding a small finite imaginary part in our calculation. We verified that this prescription has no influence on the obtained results for the real part of the $\Sigma$ s.p. potential. However, we cannot calculate the imaginary part of $U_\Sigma$. In any case, it is known that the imaginary part can be only determined reliably when using the continuous choice for the intermediate spectrum [15] and we plan to perform such a calculation in the future [40]. In the present work (like before in [37]), the nucleon s.p. potential $U_N$ is taken from a calculation [41] of pure nuclear matter employing a phenomenological $NN$ potential. It has been found that the results for the $\Lambda$ and $\Sigma$ hyperon in nuclear matter for the gap choice are not too sensitive to the choice of $U_N$ [37]. Nonetheless, also this limitation will be avoided in the future calculation [40].

In order to relate the strength of the Λ-nuclear spin-orbit potential to the two-body Λ$N$ interaction we consider the Scheerbaum factor $S_Y$ [31] calculated in nuclear matter. In the Scheerbaum approximation, the Λ- or Σ-nuclear spin-orbit potential is represented by

$$U_Y^{\ell s}(r) = -\frac{\pi}{2} S_Y \frac{1}{r} \frac{d\rho(r)}{dr} \boldsymbol{\ell} \cdot \boldsymbol{\sigma}, \tag{15}$$

with $\rho(r)$ the nucleon density distribution and $\boldsymbol{\ell}$ the single-particle orbital angular momentum operator. We adopt here the definition as given in Ref. [30]. The explicit expression for the Scheerbaum factor $S_Y$ derived in this reference in terms of the $G$-matrix elements given in momentum space reads in our notation

$$S_Y(p_Y) = -\frac{3\pi}{4(k_F)^3}\, \xi_Y (1+\xi_Y)^2 \sum_{I_0,J} \frac{2I_0+1}{(2I_Y+1)} (2J+1) \int_0^{p_{max}} \frac{d\,p}{(2\pi)^3}\, W(p,p_Y) \Big\{ (J+2)\, G^{J,I_0}_{Y1\,J+1,\,Y1\,J+1}(p,p;p_Y) + G^{J,I_0}_{Y1J,Y1J}(p,p;p_Y) - (J-1)\, G^{J,I_0}_{Y1\,J-1,\,Y1\,J-1}(p,p;p_Y) - \sqrt{J(J+1)} \Big[ G^{J,I_0}_{Y1J,Y0J}(p,p;p_Y) + G^{J,I_0}_{Y0J,Y1J}(p,p;p_Y) \Big] \Big\} \ . \tag{16}$$

## 3. The hyperon-nucleon interaction in chiral EFT

A comprehensive description of the derivation of the chiral baryon-baryon potentials for the strangeness sector using the Weinberg power counting can be found in Refs. [4, 24, 42, 43]. The LO potential consists of four-baryon contact terms without derivatives and of one-pseudoscalar-meson exchanges while at NLO contact terms with two derivatives arise, together with contributions from (irreducible) two-pseudoscalar-meson exchanges. The contributions from pseudoscalar-meson exchanges ($\pi$, $\eta$, $K$) are completely fixed by the assumed SU(3) flavor symmetry in terms of the $F$ and $D$ couplings. On the other hand, the strength parameters associated with the contact terms, the LECs, need to be determined by a fit to data. How this is done is described in detail in Ref. [4] and, therefore, we will be brief here. Since SU(3) symmetry is also imposed for the contact terms, the number of independent LECs that can contribute is significantly reduced. In particular, for the Λ$N$–Σ$N$ system there are in total 13 LECs entering the $S$-waves and the $S$–$D$ transitions, respectively, and 10 constants in the $P$-waves. The $S$-wave LECs could be fixed by a fit to available low-energy total cross sections for the reactions $\Lambda p \to \Lambda p$, $\Sigma^- p \to \Lambda n$, $\Sigma^- p \to \Sigma^0 n$, $\Sigma^- p \to \Sigma^- p$, and $\Sigma^+ p \to \Sigma^+ p$. Information from the nucleon-nucleon ($NN$) sector was not needed. The limited number (and quality) of differential cross sections and the complete lack of polarization observables makes a determination of the contact terms in the $P$-waves from Λ$N$–Σ$N$ data alone impossible. Therefore, in this case $NN$ $P$-wave phase shifts had to be used as a further constraint for the contact terms. The LEC that generates the antisymmetric spin-orbit force, and which produces a $^1P_1$-$^3P_1$ transition, was set to zero because it could not be determined from the $YN$ scattering data.

The reaction amplitudes are obtained from the solution of a coupled-channel Lippmann-Schwinger (LS) equation for the interaction potentials [4]. The potentials in the LS equation are cut off with a regulator function, $f_R(\Lambda) = \exp\left[-\left(p'^4 + p^4\right)/\Lambda^4\right]$, in order to remove high-energy components [44]. In Ref. [4] cutoff values in the range $\Lambda = 450$ – 700 MeV are considered, similar to what was used for chiral $NN$ potentials [44]. The variation of the results with the cutoff can be viewed as a rough estimate for the theoretical uncertainty [44].

As demonstrated in Ref. [4], the available Λ$N$ and Σ$N$ scattering data are very well described by the EFT interaction. Indeed the description of the $YN$ system achieved at NLO is on the same level of quality as the one by the most advanced meson-exchange $YN$ interactions. Besides an excellent description of the $YN$ data the chiral EFT interaction yields a satisfactory value for the hypertriton binding energy, see Ref. [4]. Calculations for the four-body hypernuclei ${}^4_\Lambda$H and ${}^4_\Lambda$He based on the EFT interactions can be found in Ref. [45].

Let us come back to the antisymmetric spin-orbit force. The general structure of the spin- and momentum-dependence of the contact terms at next-to-leading order is given by [4]

$$\begin{aligned} V_{YN\to YN} &= C_1 \mathbf{q}^2 + C_2 \mathbf{k}^2 + (C_3 \mathbf{q}^2 + C_4 \mathbf{k}^2)\, \boldsymbol{\sigma}_1 \cdot \boldsymbol{\sigma}_2 + \frac{i}{2} C_5 (\boldsymbol{\sigma}_1 + \boldsymbol{\sigma}_2) \cdot (\mathbf{q} \times \mathbf{k}) \\ &+ C_6 (\mathbf{q} \cdot \boldsymbol{\sigma}_1)(\mathbf{q} \cdot \boldsymbol{\sigma}_2) + C_7 (\mathbf{k} \cdot \boldsymbol{\sigma}_1)(\mathbf{k} \cdot \boldsymbol{\sigma}_2) + \frac{i}{2} C_8 (\boldsymbol{\sigma}_1 - \boldsymbol{\sigma}_2) \cdot (\mathbf{q} \times \mathbf{k}) \,, \end{aligned} \tag{17}$$

where $C_i$ ($i = 1, \ldots, 8$) are the LECs. The transferred and average momenta, $\mathbf{q}$ and $\mathbf{k}$, are defined in terms of the final and initial center-of-mass momenta of the baryons, $\mathbf{p}'$ and $\mathbf{p}$, as $\mathbf{q} = \mathbf{p}' - \mathbf{p}$ and $\mathbf{k} = (\mathbf{p}' + \mathbf{p})/2$.

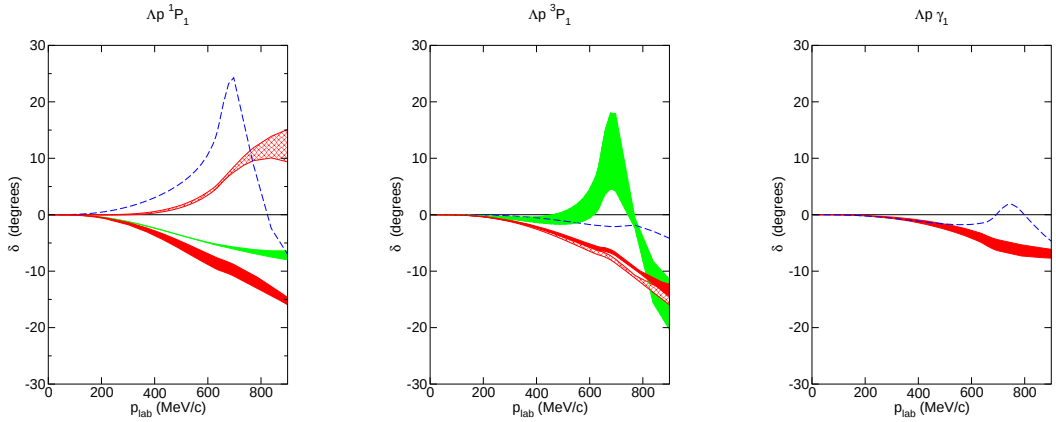


Figure 1: The $\Lambda p$ $^1P_1$ and $^3P_1$ phase shifts and the $^1P_1$–$^3P_1$ mixing parameter $\gamma_1$ as a function of $p_{\rm lab}$. The red/dark band shows the chiral EFT results to NLO for variations of the cutoff in the range $\Lambda = 500,\ldots,650$ MeV, while the green/light band are results to LO for $\Lambda = 550,\ldots,700$ MeV. The hatched band is the NLO fit from [4] without antisymmetric spin-orbit force. The dashed curve is the result of the Jülich '04 meson-exchange potential [48].

The term proportional to $C_8$ in Eq. (17) represents an antisymmetric spin-orbit force and gives rise to (spin) singlet-triplet ($^1P_1 - {}^3P_1$) transitions. After performing a partial-wave projection and imposing SU(3) symmetry constraints the $^1P_1$-$^3P_1$ transition potentials read in the notation of Ref. [4]

$$\begin{aligned}
V^{I=1/2}_{\Lambda N\to\Lambda N}(^1P_1 \to {}^3P_1) &= -C^{8_s8_a}\, p\, p' \,, \\
V^{I=1/2}_{\Lambda N\to\Sigma N}(^1P_1 \to {}^3P_1) &= -3C^{8_s8_a}\, p\, p' \,, \\
V^{I=1/2}_{\Lambda N\to\Sigma N}(^3P_1 \to {}^1P_1) &= \phantom{-}C^{8_s8_a}\, p\, p' \,, \\
V^{I=1/2}_{\Sigma N\to\Sigma N}(^1P_1 \to {}^3P_1) &= \phantom{-}3C^{8_s8_a}\, p\, p' \,, \\
V^{I=1/3}_{\Sigma N\to\Sigma N}(^1P_1 \to {}^3P_1) &= \phantom{-}0 \,,
\end{aligned} \tag{18}$$

with $p = |\mathbf{p}\,|$ and $p' = |\mathbf{p}\,'|$. Expressions for the time-reversed transitions follow from the requirement of time-reversal invariance. The superscript $8_s8_a$ of the LEC is a reminder that the singlet-triplet transition is accompanied by a transition between the symmetric and antisymmetric SU(3) octet representations as required by the generalized Pauli principle. Note that, in line with Ref. [43], we have absorbed here the overall factor $1/\sqrt{20}$ (see Table 1 in Ref. [4]) into the definition of $C^{8_s8_a}$.

In the present work we fix the LEC $C^{8_s8_a}$ by considering the Scheerbaum factor $S_\Lambda$ [31] calculated from the $G$-matrix. With regard to its "empirical" value we took studies of the splitting of the $5/2$ and $3/2$ states of $^9_\Lambda$Be by Hiyama et al. [26] and Fujiwara et al. [47] as guideline. The results of those authors suggest that values for $S_\Lambda$ in the order of $-4.6$ to $-3.0$ MeV fm$^5$ would be needed to reproduce the experimentally observed small level splitting [46]. Values of around $-3.2$ and $-4.1$ MeV fm$^5$ are suggested in Refs. [25] and [29], respectively. Since the precise value required for the $\Lambda$ s.p. spin-orbit strength can only be pinned down via a dedicated calculation of finite hypernuclei based on our EFT interactions, which is beyond the scope of the present study, we decided to aim at a typical result of $-3.7$ MeV fm$^5$. Indeed, any reference value at the expected order of magnitude would be sufficient for the main goal of the present investigation, namely for exploring in how far the LEC $C^{8_s8_a}$ can be used to achieve a small $\Lambda$ s.p. spin-orbit potential.

Of course, while introducing a non-zero contact term for the antisymmetric spin-orbit force into our EFT interaction, we still want to maintain the excellent description of the $\Lambda N$ and $\Sigma N$ scattering data as reflected in the total $\chi^2$ of only 16 – 17 for the 36 data points considered in Ref. [4]. It turned out that this is easily possible and no refit of the $S$-wave LECs is required. However, we had to re-adjust some LECs in the $^1P_1$ partial wave in order to preserve the

Table 1: The $YN$ contact terms for the $^1P_1$ partial wave and the $^1P_1$–$^3P_1$ transition potential for various cut–offs. The values of the LECs are in $10^4$ GeV$^{-4}$, the values of $\Lambda$ in MeV.

| $\Lambda$ | | 450 | 500 | 550 | 600 | 650 | 700 |
|---|---|---|---|---|---|---|---|
| $^1P_1$ | $C^{10}_{^1P_1}$ | 0.49 | 0.49 | 0.49 | 0.49 | 0.49 | 0.49 |
| | $C^{10^*}_{^1P_1}$ | −0.14 | −0.14 | −0.14 | −0.14 | −0.14 | −0.14 |
| | $C^{8_a}_{^1P_1}$ | −0.05 | −0.15 | −0.18 | −0.21 | −0.23 | −0.25 |
| $^1P_1$-$^3P_1$ | $C^{8_s 8_a}$ | −0.084 | −0.073 | −0.065 | −0.059 | −0.053 | −0.048 |

reproduction of the trend shown by the $\Sigma^- p \to \Lambda n$ differential cross sections at $p_{\rm lab} = 135 - 160$ MeV/c, cf. Fig. 4 of Ref. [4]. This resulted in a change of the sign of the predicted $\Lambda p$ $^1P_1$ phase shift. Corresponding results are shown in Fig. 1 where also the $^1P_1$–$^3P_1$ mixing parameter $\gamma_1$ is presented.

The relevant LECs are summarized in Table 1. All other LECs are kept as given in Table 3 of Ref. [4]. In this context let us mention, however, that unfortunately there is a typo in the latter table. The values for $\tilde{C}^{10}_{^3S_1}$ should read 0.104, 0.541, 1.49, 3.44, 4.99, and 5.60 for increasing cutoffs, i.e. the comma was misplaced in case of the last 4 entries. In the following we discuss NLO results for cutoffs in the range of 500–650 MeV for which the best results for $\Lambda N$ and $\Sigma N$ scattering were achieved [4].

## 4. Results

Let us now discuss the properties of our $YN$ interactions in nuclear matter. As already said, we performed a conventional $G$-matrix calculation based on the standard (gap) choice for the intermediate spectrum. Table 2 summarizes the results for the $\Lambda$ potential depth, $U_\Lambda(p_\Lambda = 0)$, evaluated at the saturation point of nuclear matter, i.e. for $k_F = 1.35$ fm$^{-1}$, obtained from our LO and NLO EFT interactions for the considered cutoff range. For illustration we include also exemplary results based on the $YN$ interaction as published in [4], i.e. without antisymmetric spin-orbit force, and, in addition, of a $YN$ interaction where all two-meson exchange contributions that involve the heavy mesons $\eta$ and/or $K$ were omitted and only the $\pi\pi$ exchange diagrams were kept, which was also considered in Ref. [4]. In this case only results for a single cutoff ($\Lambda = 650$ MeV and $\Lambda = 600$ MeV, respectively) are presented. Results obtained for the Jülich meson-exchange potentials from 2004 [48] and 1994 (model $\tilde{A}$) [37] and for the Nijmegen NSC97f model [15] are also presented. Some in-medium results for the Jülich potentials have been published before [37, 49, 50].

As can be seen from the contributions to the various partial waves, there is a moderate cutoff dependence at LO and NLO. Indeed, the variations at NLO are slightly larger than those at LO – contrary to the trend we observed for $YN$ scattering in free space [4] and for the binding energies of light hypernuclei [45]. Comparing our results at NLO with those at LO one notices that the former provides more attraction in the $^1S_0$ partial wave but significantly less in the coupled $^3S_1$–$^3D_1$ partial wave. Indeed the contribution predicted at NLO for this state is also much smaller than the values suggested by the Jülich meson-exchange potentials and other phenomenological models [15, 17, 18, 22]. We believe that this has to do with a characteristic feature of our EFT interactions that was already emphasized in Ref. [4]: The $\Lambda p$ $T$-matrix for the $^3S_1 \leftrightarrow {}^3D_1$ transition is rather large and, specifically, of the same magnitude as the ones for $^3S_1 \to {}^3S_1$ and $^3D_1 \to {}^3D_1$ at energies around the $\Sigma N$ threshold. While all three amplitudes contribute to the $\Lambda p$ cross section, the corresponding off-diagonal element of the $G$-matrix does not enter into the evaluation of $U_\Lambda$, see Eq. (12). The $P$-wave contributions generated by the LO and NLO interactions are of comparable magnitude. However, the $^3P_0$ contribution changes sign and is repulsive in the NLO case. Note that at LO there are no contact terms in the $P$-waves and, therefore, their contributions are determined solely by one-meson exchange ($\pi$, $K$, $\eta$). The partial wave contributions obtained for the NLO interaction of Ref. [4] are practically identical to those predicted by the present interaction that includes an antisymmetric spin-orbit force, cf. NLO$^\dagger$(650) versus NLO (650) in Table 2, with the exception that the strengths provided by the $^1P_1$ and $^3P_1$ partial waves are interchanged.

In lowest order of the hole-line expansion $U_\Lambda(p_\Lambda = 0)$ has to be compared with the 'empirical' value for the $\Lambda$ binding energy in nuclear matter of about −28 MeV, deduced from the binding energies of finite $\Lambda$ hypernuclei [51, 52]. The results for our EFT interactions, given in the last column of Table 2, are in good qualitative agreement

Table 2: Partial-wave contributions to $U_\Lambda(p_\Lambda = 0)$ (in MeV) at $k_F = 1.35$ fm$^{-1}$ for the LO and NLO interactions for various cutoffs. NLO$^\dagger$(650) are results based on the interaction as published in Ref. [4]. NLO (600$^*$) denotes result for an interaction where all two-meson-exchange contributions involving the $\eta$- and/or $K$ meson have been omitted, cf. text.

| | $^1S_0$ | $^3S_1 + ^3D_1$ | $^3P_0$ | $^1P_1$ | $^3P_1$ | $^3P_2 + ^3F_2$ | Total |
|---|---|---|---|---|---|---|---|
| LO (550) | −12.5 | −26.6 | −1.6 | 1.5 | 1.8 | −0.3 | −38.0 |
| LO (600) | −12.0 | −25.4 | −1.7 | 1.5 | 1.8 | −0.4 | −36.5 |
| LO (650) | −11.6 | −24.3 | −1.8 | 1.5 | 1.7 | −0.4 | −35.2 |
| LO (700) | −11.6 | −23.1 | −1.9 | 1.5 | 1.6 | −0.5 | −34.4 |
| NLO (500) | −15.3 | −15.8 | 1.1 | 2.3 | 1.1 | −1.3 | −28.2 |
| NLO (550) | −13.9 | −12.5 | 1.0 | 2.1 | 1.0 | −1.2 | −23.8 |
| NLO (600) | −12.6 | −12.0 | 0.9 | 1.9 | 0.8 | −1.1 | −22.4 |
| NLO (650) | −11.6 | −13.4 | 0.8 | 1.8 | 0.7 | −1.1 | −23.2 |
| NLO$^\dagger$(650) | −11.6 | −13.4 | 0.8 | 0.4 | 1.6 | −1.1 | −23.5 |
| NLO (600$^*$) | −12.5 | −15.9 | −0.1 | 1.1 | 1.1 | 0.6 | −26.0 |
| Jülich '04 | −10.2 | −36.3 | −0.7 | −0.6 | 0.5 | −3.2 | −51.2 |
| Jülich '94 | −3.6 | −27.2 | 0.6 | 0.7 | 1.4 | −0.8 | −29.8 |
| NSC97f | −14.6 | −23.1 | 0.5 | 2.4 | 4.6 | −0.8 | −32.4 |

with this value. One should keep in mind that, at this order of the hole-line expansion, the result depends somewhat on the choice of the single-particle potentials, see Ref. [15] for example, so that only a comparison on a qualitative level is meaningful.

Predictions for the density dependence of the Λ s.p. potential are presented in Fig. 2 where $U_\Lambda(p_\Lambda = 0)$ is shown as a function of $k_F$ for the various interactions. Obviously the EFT interaction at NLO exhibits a relatively weak density dependence as compared to that of the LO interaction and also to the Jülich '04 potential. Again, most likely this is due to the strong tensor coupling in the $^3S_1$–$^3D_1$ partial wave in combination with the $\Lambda N$–$\Sigma N$ coupling already discussed above. Interestingly, one observes an onset of repulsive effects already at rather moderate densities. Other potentials, like the NSC97f model, exhibit such a behavior too but only at somewhat higher densities [17]. The result based on the NLO interaction from [4] without antisymmetric spin-orbit component coincides more or less with the present one with an antisymmetric spin-orbit force.

Results for the Λ-nuclear spin-orbit potential, given in form of the Scheerbaum factor $S_\Lambda$ calculated in nuclear matter, see Eqs. (15)-(16), are summarized in Table 3. Besides the total $S_\Lambda$ we list also the contributions of the individual partial waves. As already said above, it has been established experimentally that the spin-orbit splitting of the Λ s.p. levels in nuclei is very small [5]. Accordingly, the Λ s.p. spin-orbit potential should also be small. In terms of the Scheerbaum factor, the value of $S_\Lambda$ required for explaining experimental data is expected to be in the order of −4.6 to −3.0 MeV fm$^5$ [46] as discussed in Sect. 3.

In Ref. [25] the Nijmegen NSC97f potential [15] and a $YN$ interaction derived within the constituent quark-model (fss2) [22] were found to predict $S_\Lambda = -15.4$ and −12.2 MeV fm$^5$ for symmetric nuclear matter at $k_F = 1.35$ fm$^{-1}$, based on a calculation where the original potentials were represented by low-momentum equivalent interactions and with the so-called continuous choice for the intermediate spectrum. Interestingly, the LO chiral EFT potential (the one with cutoff mass 600 MeV), considered also in that work, yielded with +4.8 not only a smaller value but even an opposite sign for the Λ s.p. spin-orbit potential. Results for the Nijmegen NSC97f potential can be also found in Ref. [15], however, for $k_F = 1.0$ fm$^{-1}$ (and based on a different definition of $S_\Lambda$). Our own results, using the LO EFT potential directly, are roughly in line with those of Ref. [25], cf. the last column in Table 3. Note that differences in the treatment of the intermediate spectrum in the propagator (gap versus continuous choice) do not influence the spin-dependent parts of the $G$-matrix interaction very much as demonstrated in Ref. [15]. In particular, since the contributions from $P$-states and higher partial waves are rather insensitive to the treatment of the intermediate spectrum, the same is the case for the Scheerbaum factor, cf. the pertinent results for NSC97f in Refs. [15] and [17]. The $S$-states are more strongly affected by the intermediate spectrum and it is well-known that the continuous choice

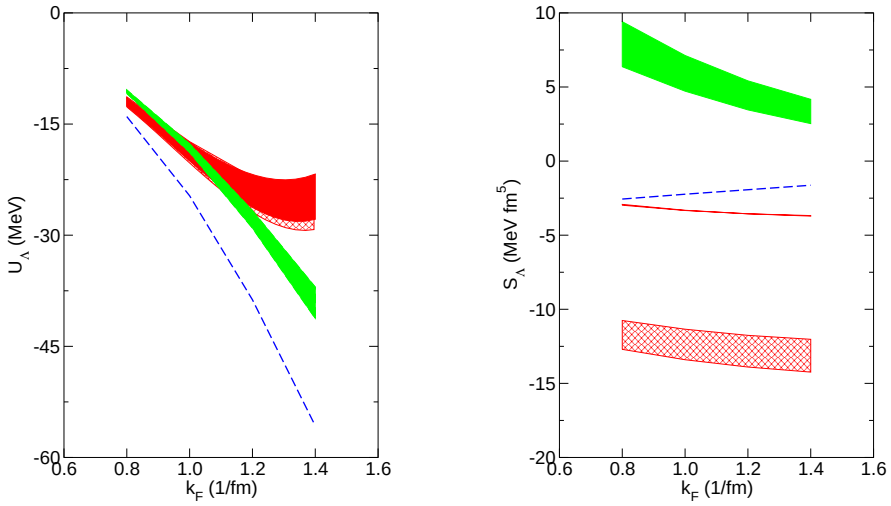


Figure 2: The Λ s.p. potential $U_\Lambda(p_\Lambda = 0)$ (left) and the Scheerbaum factor $S_\Lambda$ (right), as a function of the Fermi momentum $k_F$. The red/dark band shows the chiral EFT results to NLO for variations of the cutoff in the range $\Lambda = 500,\ldots,650$ MeV, while the green/light band are results to LO for $\Lambda = 550,\ldots,700$ MeV. The hatched band is the NLO fit from [4] without antisymmetric spin-orbit force. The dashed curve is the result of the Jülich '04 meson-exchange potential [48].

leads to a more attractive $G$-matrix interaction resulting in a 10–20 % increase of $U_\Lambda$ at $p_\Lambda = 0$ as compared to the gap choice (see, e.g., Ref. [15]).

For the NLO potential we obtain $S_\Lambda = -3.7$ MeV fm$^5$, as aimed at in the fitting procedure. It is interesting to compare the new NLO results with the ones based on the original NLO interaction [4], i.e. the one without antisymmetric spin-orbit force. Corresponding predictions, exemplary for $\Lambda = 650$ MeV, are included also in Table 3 and denoted by NLO$^\dagger$(650). Clearly in this case $S_\Lambda$ is significantly larger. A closer inspection of the respective partial-wave contributions reveals what one expects anyway, namely that the main difference is due to the antisymmetric spin-orbit force whose contribution is given in the column labelled with $^1P_1 \leftrightarrow {}^3P_1$. It is zero for the LO interaction (because there is no antisymmetric spin-orbit force at that order) and also for the original NLO interaction, where it has been assumed to be zero. With the corresponding contact term included its strength can be used to counterbalance the sizeable spin-orbit force generated by the basic interaction so that the small $S_\Lambda$ is then achieved by a cancellation between the spin-orbit and antisymmetric spin-orbit components of the $G$-matrix interaction.

Note, however, that the results in Table 3 indicate that such a cancellation is not the only mechanism that can provide a small spin-orbit force. For example, let us look at the predictions for the interaction (denoted by) NLO (600$^*$), where all two-meson-exchange contributions involving the $\eta$- and/or $K$ meson have been omitted. Here, a very small $S_\Lambda$ is achieved without any antisymmetric spin-orbit force. It is simply due to overall more repulsive contributions, notably in the $^3P_0$ and $^3P_2$ partial waves. We want to emphasize that the interaction NLO (600$^*$) reproduces all $\Lambda N$ and $\Sigma N$ scattering data with the same high quality as the other EFT interactions at NLO, see the results in Ref. [4]. It is worthwhile to mention that also the Jülich meson-exchange potentials predict rather small values for the Scheerbaum factor. For both interactions there is a substantial contribution from the antisymmetric spin-orbit force which is primarily due to vector-meson ($\omega$) exchange [37]. The magnitude is comparable to the one of the chiral EFT interaction at NLO. Finally, we want to draw attention to a recent lattice QCD calculation dealing with the $\Lambda N$ spin-orbit force [54]. In this work only a weak cancellation between the spin-orbit and antisymmetric spin-orbit potentials is obtained. However, one has to keep in mind that the calculation is performed in the (flavor) SU(3) limit and, specifically, for quark masses far away from their physical values.

Table 3: Partial-wave contributions to the Scheerbaum factor $S_\Lambda$ (in MeV fm$^5$). Same description of interactions as in Table 2.

| | $^3P_0$ | $^3D_1$ | $^3P_1$ | $^1P_1 \leftrightarrow {}^3P_1$ | $^3P_2$ | $^3D_2$ | $^3D_3$ | Total |
|---|---|---|---|---|---|---|---|---|
| LO (550) | 8.7 | −0.2 | −5.2 | 0.0 | −0.9 | 0.4 | −0.1 | 2.7 |
| LO (600) | 9.3 | −0.2 | −5.0 | 0.0 | −1.1 | 0.4 | −0.1 | 3.3 |
| LO (650) | 9.8 | −0.2 | −4.8 | 0.0 | −1.2 | 0.4 | −0.1 | 3.8 |
| LO (700) | 10.4 | −0.2 | −4.7 | 0.0 | −1.4 | 0.4 | −0.1 | 4.4 |
| NLO (500) | −5.9 | −0.6 | −3.3 | 8.9 | −3.4 | 0.4 | 0.2 | −3.7 |
| NLO (550) | −5.2 | −0.6 | −2.8 | 7.5 | −3.1 | 0.4 | 0.2 | −3.7 |
| NLO (600) | −4.8 | −0.6 | −2.4 | 6.6 | −3.0 | 0.4 | 0.2 | −3.7 |
| NLO (650) | −4.4 | −0.6 | −2.0 | 5.8 | −3.0 | 0.4 | 0.2 | −3.7 |
| NLO$^\dagger$(650) | −4.4 | −0.6 | −4.6 | 0.0 | −3.0 | 0.4 | 0.2 | −12.0 |
| NLO (600$^*$) | 0.5 | −0.1 | −3.2 | 0.0 | 1.7 | 0.5 | 0.1 | −0.5 |
| Jülich '04 | 4.0 | 0.5 | −1.3 | 4.6 | −9.2 | 0.6 | −1.0 | −1.7 |
| Jülich '94 | −3.3 | 1.2 | −3.8 | 8.4 | −2.5 | 0.6 | −1.3 | −0.4 |
| NSC97f | −2.2 | 0.2 | −12.7 | 2.3 | −2.6 | −1.0 | −1.9 | −15.6 |

The dependence of $S_\Lambda$ on $k_F$ can be seen in Fig. 2. Obviously, except for the LO interaction, the density dependence is fairly weak. A weak density dependence of $S_\Lambda$ was also observed in Ref. [22] in a calculation of the Scheerbaum factor for a $YN$ interaction based on the quark model, and likewise for the Nijmegen $YN$ potentials [15].

Let us now come to the Σ hyperon. In the course of constructing the NLO EFT interaction [4] it turned out that the available $YN$ scattering data can be fitted equally well with an attractive or a repulsive interaction in the $^3S_1$ partial wave of the $I = 3/2$ $\Sigma N$ channel. Indeed the underlying SU(3) structure as given in Table 1 of Ref. [4] suggests that there should be some freedom in choosing the interaction in this particular partial wave. From that table one can see that the $^3S_1$ partial wave in the $I = 3/2$ $\Sigma N$ channel belongs to the "isolated" 10 representation so that the corresponding contact interaction does not enter into any of the interactions in the other $YN$ channels. Since a repulsive Σ-nuclear potential can only be achieved with a repulsive $^3S_1$ interaction in the $I = 3/2$ channel, as already discussed in the Introduction, the freedom mentioned above can be used to control the properties of the Σ in nuclear matter within the EFT approach.

The NLO interaction presented in Ref. [4] produces a moderately repulsive $^3S_1$ phase shift as can be seen in Fig. 9 in Ref. [4]. A comparable repulsion is also predicted by the LO potential. For the latter, calculations of the Σ single-particle potential have been performed [25] and indicated values of $U_\Sigma(p_\Sigma = 0) \approx 12$ MeV at nuclear matter saturation density. Results for our (LO and NLO) EFT interactions, obtained in the present calculation, are compiled in Table 3. First we note that again our own LO results are roughly in line with those reported by Kohno [25], considering, of course, the different prescriptions used for the treatment of the intermediate spectrum in the propagator. The Σ potential depth predicted at LO and NLO is of comparable magnitude and amounts to a repulsion in the order of 15 to 20 MeV. There is a considerable cutoff dependence visible in the LO results which is, however, noticeably reduced at the NLO level. The Jülich meson-exchange potentials, but also the Nijmegen NSC97f interaction, yield an attractive Σ s.p. potential as can be seen from Table 4. Note that the Jülich '04 interaction actually predicts a repulsive $^3S_1$ partial wave in the $I = 3/2$ $\Sigma N$ channel, see the phase shifts in Fig. 9 of Ref. [4]. However, it is not strong enough to overcome the attraction provided by most of the other partial wave contributions, cf. Table 4. The Jülich '94 interaction produces an unphysical (quasi) bound state in the $^1S_0$ partial wave of the $I = 1/2$ $\Sigma N$ channel, visible as a broad shoulder in the $\Lambda p$ cross section at around $p_{lab} \approx 350$ MeV/c, cf. Refs. [37, 53]. As a consequence of this there is a large attractive contribution of this partial wave to $U_\Sigma$ and the total $U_\Sigma^0$ is also large and attractive.

A recent overview by Gal [6] of results from various phenomenological analyses of data on $\Sigma^-$ atoms [13, 14] and $(\pi^-, K^+)\Sigma$ spectra [11, 12] gives a range of 10-50 MeV for the isoscalar part of the Σ s.p. potential and $\simeq +80$ MeV for the isovector component. The predictions of the EFT interactions are well in line with those values. Obviously, there is a large uncertainty with regard to the actual strength of the isoscalar part needed for describing the data. Our

EFT results are more at the lower end of the inferred range. It should be said, however, that significantly larger values are difficult to achieve. As already pointed out in [4], there is not that much freedom to accommodate more repulsion. Specifically, a more strongly repulsive $^3S_1$ phase shift in the $I = 3/2$ $\Sigma N$ channel, as suggested for example by recent lattice QCD calculations [55], would lead to a sizeable increase in the $\Sigma^+ p$ cross section, in excess of what is required to describe the available data, and accordingly would result in a dramatic deterioration of the achieved $\chi^2$. For the same reason it would be practically impossible to realize values for the (isoscalar) $\Sigma$ s.p. potential in the order of 60 MeV, as suggested by the perturbative calculation in [33].

Interestingly, the Scheerbaum factor $S_\Sigma$ is of comparable magnitude for all interactions considered. Like in the $\Lambda$ case, the LO EFT interaction predicts an opposite sign for this quantity. Note that there are no experimental constraints on the value of $S_\Sigma$ so far.

Table 4: Partial-wave contributions to $U_\Sigma(0)$ (in MeV). Total results for the isoscalar ($U_\Sigma^0$) and isovector ($U_\Sigma^1$) decomposition according to Eq. (14) and for the Scheerbaum factor $S_\Sigma$ (in MeV fm$^5$) are given as well. Same description of interactions as in Table 2.

| | Isospin $I_0 = 1/2$ | | | Isospin $I_0 = 3/2$ | | | | | |
|---|---|---|---|---|---|---|---|---|---|
| | $^1S_0$ | $^3S_1$+$^3D_1$ | $P$ | $^1S_0$ | $^3S_1$+$^3D_1$ | $P$ | $U_\Sigma^0$ | $U_\Sigma^1$ | $S_\Sigma$ |
| LO (550) | 8.0 | −15.2 | −2.7 | −9.9 | 49.1 | −0.8 | 28.0 | 60.8 | 8.4 |
| LO (600) | 8.5 | −16.2 | −3.2 | −10.0 | 44.6 | −1.0 | 22.1 | 58.1 | 9.9 |
| LO (650) | 8.6 | −17.1 | −3.7 | −10.0 | 40.2 | −1.2 | 16.2 | 56.4 | 11.4 |
| LO (700) | 8.1 | −18.0 | −4.3 | −9.8 | 37.0 | −1.3 | 11.1 | 57.0 | 13.1 |
| NLO (500) | 6.9 | −22.5 | 3.4 | −11.4 | 39.3 | −0.2 | 14.8 | 54.6 | −17.9 |
| NLO (550) | 6.3 | −23.6 | 2.5 | −10.8 | 43.8 | −0.2 | 17.3 | 64.9 | −16.4 |
| NLO (600) | 5.0 | −23.3 | 1.8 | −10.2 | 42.5 | −0.2 | 14.8 | 67.8 | −14.8 |
| NLO (650) | 4.4 | −22.3 | 1.3 | −9.6 | 39.1 | −0.3 | 11.9 | 65.0 | −14.1 |
| NLO$^\dagger$(650) | 4.4 | −22.3 | 1.7 | −9.7 | 39.1 | −0.4 | 12.2 | 64.1 | −9.3 |
| NLO (600$^*$) | 6.7 | −25.9 | 3.4 | −10.5 | 45.2 | −0.2 | 18.0 | 68.9 | −5.5 |
| Jülich '04 | 4.2 | −15.1 | −8.2 | −12.0 | 11.7 | −2.0 | −22.2 | 38.0 | −13.3 |
| Jülich '94 | −18.0 | −19.5 | −5.1 | −7.7 | −15.8 | −4.1 | −71.4 | 59.1 | −19.8 |
| NSC97f | 15.0 | −8.8 | 0.5 | −12.6 | −6.4 | −2.6 | −16.1 | −32.8 | −15.8 |

## 5. Summary

We have investigated the in-medium properties of a hyperon-nucleon potential, derived within chiral effective field theory and fitted to low-energy $\Lambda N$ and $\Sigma N$ scattering data. In particular, we have evaluated the single-particle potential for the $\Lambda$ and $\Sigma$ hyperons in nuclear matter in a conventional $G$-matrix calculation, and the Scheerbaum factor associated with the hyperon-nucleus spin-orbit interaction. Results are presented for a leading-order interaction published in 2006 which accounts well for the bulk properties of the $\Lambda N$ and $\Sigma N$ system [24] and for our recent $YN$ interaction derived up to next-to-leading order in chiral EFT which provides an excellent description of the available $YN$ data [4].

The predictions for the $\Lambda$ single-particle potential turned out to be in good qualitative agreement with the empirical values inferred from hypernuclear data. A depth of about −25 MeV is found for the NLO interaction and of about −36 MeV for the LO potential. The $\Sigma$-nuclear potential is found to be repulsive, in agreement with phenomenological information, with values around 15–20 MeV.

Empirical information suggests that the $\Lambda$-nucleus spin-orbit interaction should be rather weak. Therefore, we discussed also the spin-orbit interaction and, in particular, the role of the antisymmetric spin-orbit force in the $YN$ system. The chiral EFT approach yields a potential that contains, besides pseudoscalar meson exchanges ($\pi$, $K$, $\eta$), a series of contact interactions with an increasing number of derivatives. In this approach a contact term representing an antisymmetric spin-orbit force arises already at NLO. It induces $^1P_1$–$^3P_1$ transitions in the coupled ($I = 1/2$) $\Lambda N$–$\Sigma N$

system. The low-energy constant associated with the contact term could not be pinned down by a fit to the existing $\Lambda N$ and $\Sigma N$ scattering data as found in [4] and, therefore, it was simply put to zero in that work. As demonstrated in the present study, it can be fixed, however, from investigating the properties of the $\Lambda$ hyperon in nuclear matter and, specifically, it can be utilized to achieve a weak $\Lambda$-nuclear spin-orbit potential. In any case, and especially with regard to the spin-orbit force, one has to acknowledge that nuclear matter calculations can provide only a first glimpse on the properties of the $YN$ interaction in the medium. A stringent test of the properties of the EFT interactions in the medium can be only performed by deducing effective interactions (from the $G$-matrix in nuclear matter) and applying them in calculations of finite hypernuclei.

## Acknowledgements

The authors acknowledge helpful communications with Avraham Gal, Norbert Kaiser, Michio Kohno and Yasuo Yamamoto. This work is supported in part by the DFG and the NSFC through funds provided to the Sino-German CRC 110 “Symmetries and the Emergence of Structure in QCD” and by the EU Integrated Infrastructure Initiative HadronPhysics3. Part of the numerical calculations has been performed on the supercomputer cluster of the JSC, Jülich, Germany.

## References

[1] S. Weinberg, Phys. Lett. B **251** (1990) 288.
[2] S. Weinberg, Nucl. Phys. B **363** (1991) 3.
[3] E. Epelbaum, H. -W. Hammer and U.-G. Meißner, Rev. Mod. Phys. **81** (2009) 1773.
[4] J. Haidenbauer, S. Petschauer, N. Kaiser, U.-G. Meißner, A. Nogga and W. Weise, Nucl. Phys. A **915** (2013) 24.
[5] O. Hashimoto and H. Tamura, Prog. Part. Nucl. Phys. **57** (2006) 564.
[6] A. Gal, Prog. Theor. Phys. Suppl. **186** (2010) 270.
[7] E. Botta, T. Bressani and G. Garbarino, Eur. Phys. J. A **48** (2012) 41.
[8] E. Friedman and A. Gal, Phys. Rept. **452** (2007) 89.
[9] H. Noumi et al., Phys. Rev. Lett. **89** (2002) 072301; **90** (2003) 049902 (E).
[10] P.K. Saha et al., Phys. Rev. C **70** (2004) 044613.
[11] M. Kohno, Y. Fujiwara, Y. Watanabe, K. Ogata and M. Kawai, Prog. Theor. Phys. **112** (2004) 895.
[12] M. Kohno, Y. Fujiwara, Y. Watanabe, K. Ogata and M. Kawai, Phys. Rev. C **74** (2006) 064613.
[13] C.J. Batty, E. Friedman and A. Gal, Phys. Lett. B **335** (1994) 273.
[14] J. Mareš, E. Friedman, A. Gal and B.K. Jennings, Nucl. Phys. A **594** (1995) 311.
[15] T. A. Rijken, V. G. J. Stoks and Y. Yamamoto, Phys. Rev. C **59** (1999) 21.
[16] I. Vidaña, A. Polls, A. Ramos, M. Hjorth-Jensen and V. G. J. Stoks, Phys. Rev. C **61** (2000) 025802.
[17] T. A. Rijken and Y. Yamamoto, Phys. Rev. C **73** (2006) 044008.
[18] T. A. Rijken and Y. Yamamoto, Nucl. Phys. A **804** (2008) 51.
[19] T. A. Rijken, M. M. Nagels and Y. Yamamoto, Prog. Theor. Phys. Suppl. **185** (2010) 14.
[20] Y. Yamamoto, T. Motoba and T. A. Rijken, Prog. Theor. Phys. Suppl. **185** (2010) 72.
[21] H.-J. Schulze and T. Rijken, Phys. Rev. C **88** (2013) 024322.
[22] Y. Fujiwara, Y. Suzuki and C. Nakamoto, Prog. Part. Nucl. Phys. **58** (2007) 439.
[23] M. Kohno, Y. Fujiwara, T. Fujita, C. Nakamoto and Y. Suzuki, Nucl. Phys. A **674** (2000) 229.
[24] H. Polinder, J. Haidenbauer and U.-G. Meißner, Nucl. Phys. A **779** (2006) 244.
[25] M. Kohno, Phys. Rev. C **81** (2010) 014003.
[26] E. Hiyama, M. Kamimura, T. Motoba, T. Yamada and Y. Yamamoto, Phys. Rev. Lett. **85** (2000) 270.
[27] D. J. Millener, Nucl. Phys. A **835** (2010) 11.
[28] D. J. Millener, J. Phys. Conf. Ser. **312** (2011) 022005.
[29] Y. Fujiwara, M. Kohno and Y. Suzuki, Mod. Phys. Lett. A **24** (2009) 1031.
[30] Y. Fujiwara, M. Kohno, T. Fujita, C. Nakamoto and Y. Suzuki, Nucl. Phys. A **674** (2000) 493.
[31] R. R. Scheerbaum, Nucl. Phys. A **257** (1976) 77.
[32] N. Kaiser and W. Weise, Phys. Rev. C **71** (2005) 015203.
[33] N. Kaiser, Phys. Rev. C **71** (2005) 068201.
[34] N. Kaiser, Phys. Rev. C **76** (2007) 068201.
[35] N. Kaiser and W. Weise, Nucl. Phys. A **804** (2008) 60.
[36] J. Martin Cámalich and M. J. Vicente Vacas, Phys. Rev. C **75** (2007) 035207.
[37] A. Reuber, K. Holinde and J. Speth, Nucl. Phys. A **570** (1994) 543.
[38] J. Dabrowski and M.Y.M. Hassan, Phys. Rev. C **1** (1970) 1883.
[39] D.M. Rote and A.R. Bodmer, Nucl. Phys. A **148** (1970) 97.
[40] S. Petschauer et al., in preparation.
[41] Y. Yamamoto, private communication.

[42] J. Haidenbauer, U.-G. Meißner, A. Nogga and H. Polinder, Lect. Notes Phys. **724** (2007) 113.
[43] S. Petschauer and N. Kaiser, Nucl. Phys. A **916** (2013) 1.
[44] E. Epelbaum, W. Glöckle and U.-G. Meißner, Nucl. Phys. A **747** (2005) 362.
[45] A. Nogga, Few Body Syst. **55** (2014) 757.
[46] M. Kohno, private communication.
[47] Y. Fujiwara, M. Kohno, K. Miyagawa and Y. Suzuki, Phys. Rev. C **70** (2004) 047002.
[48] J. Haidenbauer and U.-G. Meißner, Phys. Rev. C **72** (2005) 044005.
[49] F. Sammarruca, arXiv:0801.0879 [nucl-th].
[50] J. Hu, E. Hiyama and H. Toki, Phys. Rev. C **90** (2014) 014309.
[51] D. J. Millener, C. B. Dover and A. Gal, Phys. Rev. C **38** (1988) 2700.
[52] Y. Yamamoto, H. Bando and J. Žofka, Prog. Theor. Phys. **80** (1988) 757.
[53] B. Holzenkamp, K. Holinde and J. Speth, Nucl. Phys. A **500** (1989) 485.
[54] N. Ishii *et al.* [HAL QCD Collaboration], PoS LATTICE **2013** (2014) 234.
[55] S. R. Beane *et al.*, Phys. Rev. Lett. **109** (2012) 172001.